CO_2 and Water Activation on Ceria Nanocluster Modified TiO_2 Rutile (110)

Stephen Rhatigan and Michael Nolan*

Tyndall National Institute, University College Cork, Lee Maltings, Cork, Ireland

michael.nolan@tyndall.ie

Supplementary Material

This document contains supplementary material relevant to the paper entitled: *"CO_2 and Water activation on Ceria Nanocluster Modified TiO_2 Rutile (110)"*.

List of Tables:

List of Figures:

METHODOLOGY

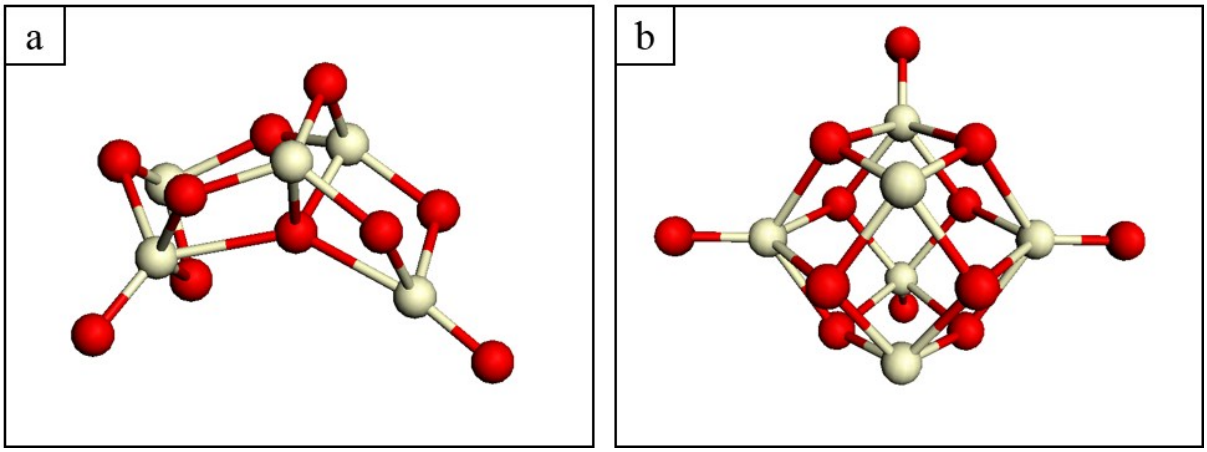

Figure S1 Relaxed atomic structures of stoichiometric gas phase nanoclusters, **(a)** Ce_5O_{10} and **(b)** Ce_6O_{12}.

The nanocluster modifiers, of compositions Ce_5O_{10} and Ce_6O_{12}, shown in Figure S1, were relaxed in the gas phase within the same computational setup described in the section 2 of the main text, with no constraints on the ionic positions. We relaxed a number of nanocluster structures and those shown in Figure S1 were the lowest energy structures that we found and are typical of the non-bulk-like structure found for this size of (predominantly) ionic oxide nanoclusters.

These low energy ceria nanoclusters were then adsorbed at the rutile (110) surface in different configurations and each of these were relaxed, as described in previous work.[1-7] The most stable $(CeO_2)_n$-rutile-(110) heterostructures were used in the subsequent calculations. Although there are many possible adsorption structures of the nanoclusters on the rutile (110) surface, with a range of adsorption energies, we find that once the nanoclusters are adsorbed in stable configurations, the trends in key properties, such as band gap reduction are unaffected.[7] For this study, we use representative CeO_x-rutile-(110) composites to examine the impact of modification on the photocatalytic properties and the interaction of CO_2 and water, and expect little significant effect due to the precise structure of the composite surface.

We model photoexcitation by imposing a triplet electronic state on the system. This promotes an electron to the conduction band, with a corresponding hole in the valence band, and enables an evaluation of the energetics and charge localization associated with photoexcitation. The following energies are computed:

- The ground state energy of the system, yielding $E^{singlet}$.
- A single point energy calculation at the ground state geometry with the triplet state imposed, yielding $E^{unrelaxed}$.
- An ionic relaxation of the triplet electronic state which gives $E^{relaxed}$.

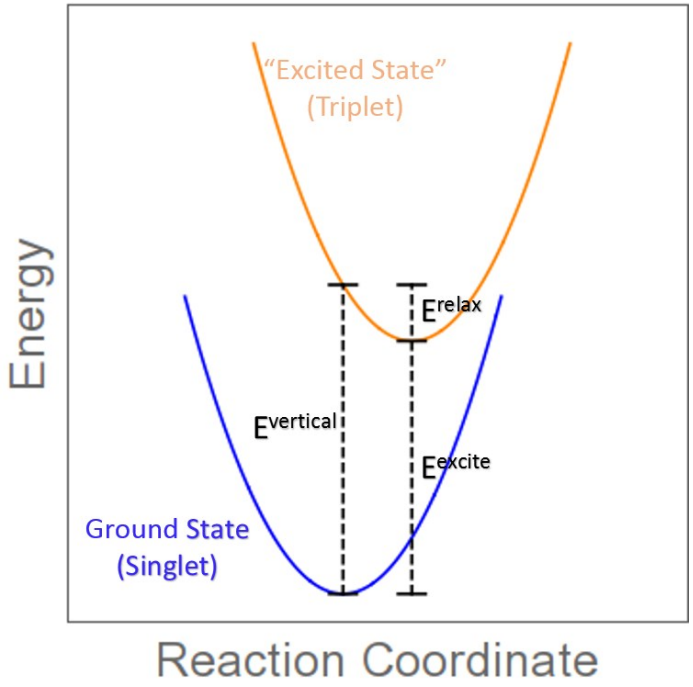

Figure S2 Schematic diagram of the relationship between the energies computed in the photoexcited model.

From the results of these calculations we compute:

1. The singlet-triplet vertical excitation energy:
$$E^{vertical} = E^{unrelaxed} - E^{singlet}$$
This is the difference in energy between the ground (singlet) state and the imposed triplet state at the singlet geometry and corresponds to the simple VB-CB energy gap from the computed density of states.

2. The singlet-triplet excitation energy:
$$E^{excite} = E^{relaxed} - E^{singlet}$$
This is the difference in energy between the relaxed triplet state and the relaxed singlet state and gives a crude approximation of the excitation energy.

3. The triplet relaxation (carrier trapping) energy:
$$E^{relax} = E^{unrelaxed} - E^{relaxed}$$

This difference in energy between the unrelaxed and relaxed triplet states is the energy gained when the electron and hole are trapped at their metal and oxygen sites upon structural relaxation. This energy relates to the stability of the trapped electron and hole.

These quantities are summarized schematically in Figure S2.

RESULTS

The following are relevant to **Section 3.1** of the main text: ***"Stoichiometric CeO_2-modified TiO_2 structures"***.

In the Ce_5O_{10}-rutile-(110) composite (Figure 1(a) of the main text), two Ce ions are coordinated to four O_C atoms; three Ce cations are five-fold coordinated and form interfacial bonds with bridging O_S ions with Ce-O distances of 2.3-2.4 Å. Each O_C ion is two-fold coordinated with the exception of one at the centre of the cluster which coordinates to three cluster cations. Three O_C ions bind to surface Ti ions with Ti-O_C distances of 1.8-2.0 Å.

For Ce_6O_{12}-rutile-(110) (Figure 1(d) of the main text), five Ce are five-fold coordinated with one four-fold coordinated Ce cation. Two cluster Ce each bind to two bridging O_S with Ce-O distances of 2.4-2.6 Å. The O_C ions bind to three metal cations with the exception of three terminal O_C which are singly coordinated to Ce ions. Ce-O distances involving singly coordinated O_C ions are 1.9 Å and compare with typical Ce-O distances in the range of 2.1-2.6 Å for the other O_C atoms. Two O_C each form a single interfacial bond with surface titanium ions with Ti-O_C distances of 1.8 Å and 1.9 Å.

The interfacial bonding between the nanocluster and the surface results in an appreciable distortion of the local atomic structure at the surface. Where a bridging O_S is bound to a nanocluster cation the Ti-O_S bond is elongated by up to 10% compared with a typical unmodified bond length of 1.88 Å. Ti atoms that bind with O_C migrate out of the surface plane towards the cluster by as much as 0.92 Å, lengthening the subsurface Ti-O distance.

The following tables are relevant to **Section 3.2** of the main text: ***"Reduction of CeO_2-rutile by oxygen vacancy formation"***.

Table S1 Computed oxygen vacancy formation energies for each O site of the supported ceria nanoclusters. The most stable vacancy sites are highlighted in bold. Values in brackets were computed with aspherical gradient corrections.

Ce_5O_{10}-rutile-(110)		**Ce_5O_9-rutile-(110)**	
O site	**E_{vac} (eV)**	**O site**	**E_{vac} (eV)**
1	1.35	1	2.96
2	2.03	2	2.95
3	1.38	3	1.86
4	1.67	4	2.03
5	2.38	5	2.38
6	**0.18 (0.02)**	6	2.30
7	1.93	**7**	**1.44 (1.33)**
8	1.53	8	1.76
9	1.56	9	2.35
10	1.65		

Ce_6O_{12}-rutile-(110)		**Ce_6O_{11}-rutile-(110)**		**Ce_6O_{10}-rutile-(110)**	
O site	**E_{vac} (eV)**	**O site**	**E_{vac} (eV)**	**O site**	**E_{vac} (eV)**
1	1.91	1	1.56	1	2.15
2	1.68	2	1.49	2	2.97
3	-0.10	**3**	**-0.16 (-0.62)**	3	3.35
4	1.68	4	1.60	4	1.98
5	1.26	5	1.03	5	2.60
6	1.62	6	1.72	6	2.02
7	0.58	7	1.56	7	2.68
8	2.81	8	2.49	8	2.89
9	3.09	9	2.01	**9**	**0.30 (0.31)**
10	0.29	10	0.14	10	5.04
11	**-0.46 (-0.26)**	11	2.40		
12	2.70				

Table S2 Ce-O distances and coordination for each of the Ce ions in the supported nanoclusters in the stoichiometric, ground state and reduced state. Reduced Ce^{3+} ions are highlighted in bold.

Stoichiometry	**Ion**	**Coord**	**Ce-O distances (Å)**					
Ce_5O_{10}	Ce_I	5	2.42	2.24	2.19	2.17	2.14	
	Ce_{II}	5	2.38	2.31	2.31	2.17	2.15	
	Ce_{III}	4	2.29	2.12	2.11	2.08		
	Ce_{IV}	5	2.44	2.29	2.24	2.16	2.15	
	Ce_V	4	2.24	2.15	2.13	2.08		
Ce_5O_9	**Ce_I**	6	2.59	2.57	2.54	2.45	2.33	2.31
	Ce_{II}	5	2.42	2.35	2.31	2.14	2.13	
	Ce_{III}	4	2.34	2.15	2.14	2.01		
	Ce_{IV}	5	2.60	2.42	2.40	2.29	2.25	
	Ce_V	4	2.25	2.14	2.12	2.08		
Ce_5O_8	**Ce_I**	5	2.57	2.56	2.40	2.29	2.22	
	Ce_{II}	5	2.54	2.53	2.38	2.31	2.25	
	Ce_{III}	4	2.34	2.13	2.09	2.07		
	Ce_{IV}	4	2.47	2.43	2.33	2.17		
	Ce_V	3	2.24	2.17	2.16			
Stoichiometry	**Ion**	**Coord**	**Ce-O distances (Å)**					
Ce_6O_{12}	Ce_I	5	2.46	2.41	2.39	2.38	1.86	
	Ce_{II}	5	2.52	2.37	2.36	2.35	1.86	
	Ce_{III}	4	2.19	2.19	2.13	2.07		
	Ce_{IV}	5	2.35	2.22	2.20	2.20	2.15	
	Ce_V	6	2.45	2.41	2.37	2.24	2.24	2.2
	Ce_{VI}	5	2.57	2.54	2.42	2.33	1.85	
Ce_6O_{10}	**Ce_I**	4	2.35	2.32	2.26	2.23		
	Ce_{II}	5	2.49	2.36	2.36	2.34	1.88	
	Ce_{III}	4	2.35	2.32	2.26	2.23		
	Ce_{IV}	5	2.48	2.36	2.31	2.30	2.28	
	Ce_V	6	2.48	2.48	2.45	2.21	2.16	2.16
	Ce_{VI}	6	2.58	2.58	2.55	2.36	2.36	2.31
Ce_6O_9	**Ce_I**	4	2.31	2.29	2.28	2.26		
	Ce_{II}	4	2.32	2.28	2.28	2.25		
	Ce_{III}	4	2.29	2.29	2.29	2.29		
	Ce_{IV}	5	2.48	2.41	2.34	2.28	2.28	
	Ce_V	6	2.57	2.56	2.51	2.34	2.33	2.32
	Ce_{VI}	6	2.60	2.58	2.56	2.37	2.33	2.32

The following Figure and analysis are relevant to **Section 3.2** of the main text: ***"Reduction of CeO_2-rutile by oxygen vacancy formation"***.

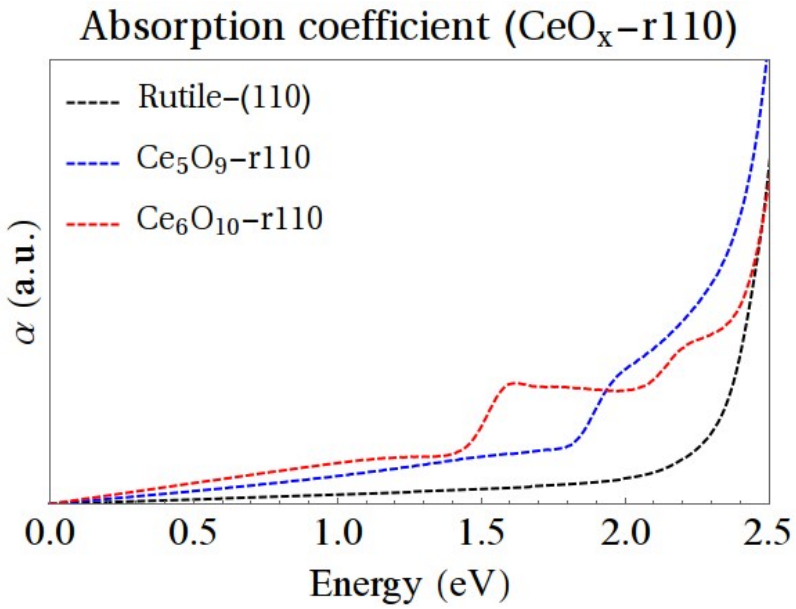

Figure S3 Computed absorption spectra for unmodified rutile (110), and the ground state heterostructures, Ce_5O_9- and Ce_6O_{10}-rutile-(110).

To complement our analysis of the DOS plots and their implications for the light absorption properties of the modified surfaces we compute the real and imaginary parts, ϵ_1 and ϵ_2, of the frequency dependent dielectric function. From this we calculate the extinction coefficient, κ, *via*:

$$\kappa = \sqrt{\frac{\sqrt{\epsilon_1^2 + \epsilon_2^2} - \epsilon_1^2}{2}}$$

and from κ, we compute the absorption coefficient:

$$\alpha = \frac{2\omega\kappa}{c}$$

where ω and c are the angular frequency and speed of light in vacuum respectively.

The computed absorption spectra for the bare rutile (110) surface and the ground states heterostructures, Ce_5O_9- and Ce_6O_{10}-rutile-(110), are shown in Figure S3. We observe the onset of light absorption at lower energies for the ceria-modified rutile structures; optical gaps are ~2.2 eV for unmodified rutile (110) and for Ce_5O_9- and Ce_6O_{10}-rutile-(110), the optical gaps are ~1.8 eV and ~1.4 eV respectively. This agrees with trends observed in the DOS plots

(Figure 3 of the main text). For Ce_5O_9-rutile-(110) (Figure 3(b)), occupied states, due to Ce^{3+} ions, in the band gap are responsible for the red shift in the absorption edge. For Ce_6O_{10}-rutile-(110) (Figure 3(e)), a combination of occupied Ce^{3+}-derived states and O_C 2p states contribute to the observed red shift. The reduced optical gap computed for Ce_6O_{10}-rutile-(110) relative to Ce_5O_{10}-rutile-(110) can be understood in regarding the insets of Figure 3(b) and 3(e); for the larger nanocluster-surface composite, the occupied Ce 4f states lie higher in energy and closer to the conduction band of the TiO_2 support.

The following Figure and analysis are relevant to **Section 3.3** of the main text: ***"Modelling charge separation upon photoexcitation"***.

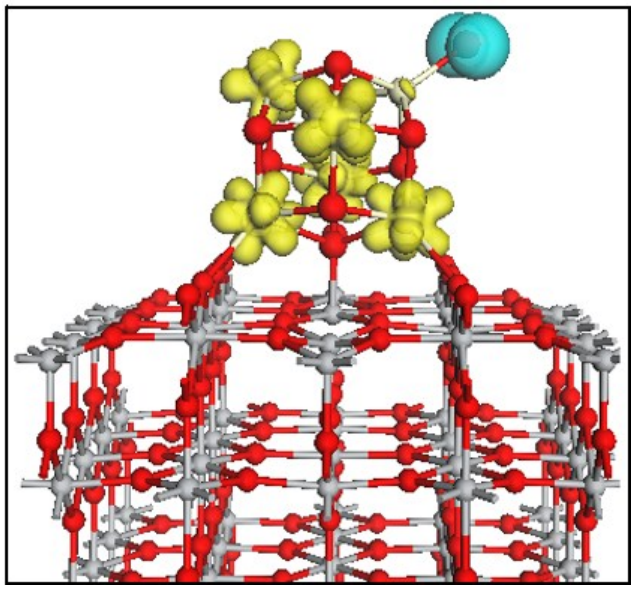

Figure S4 Spin density plots for the photoexcited electron and hole in Ce_6O_{10}-rutile-(110). The spin density isosurfaces are yellow for electrons and blue for holes and enclose spin densities of up to 0.02 eV/Å^3.

For the photoexcited model applied to the Ce_6O_{10}-rutile-(110) composite, shown in Figure S4, there are five unpaired electrons; four are due to the formation of two neutral oxygen vacancies and are localized at Ce_I, Ce_{III}, Ce_{IV} and Ce_V (compare with Figure 2(c) of main text). The fifth photoexcited electron localizes at Ce_V; Ce_V maintains a six-fold coordination, and the Ce-O distances increase by up to 10% relative to their values in the ground state. In the Ce_6O_{10}-rutile-(110) system the hole localizes at a singly coordinated terminal oxygen site; the Ce-O distance increases from 1.9 Å in the ground state to 2.3 Å after excitation. Hole localization is accompanied by a change in the computed Bader charge of the oxygen by 0.4 electrons, from 7.1 to 6.7 electrons. A spin magnetization of 0.78 μ_B was computed for the singly terminated oxygen site at which the hole localizes in Ce_6O_{10}-rutile-(110).

The following Figures and analysis are relevant to **Section 3.4** of the main text: ***"H_2O adsorption at the reduced nanocluster-surface composites"***

For the reduced Ce_6O_9 nanocluster, the O sites (Ce sites) show three-fold (four-fold) or higher coordination. The water molecule dissociates upon adsorption with transfer of an H atom to an O_C site and the OH group binding to a single neighbouring Ce ion (Figures 5(c) and 5(d) of the main text). The O_C and Ce adsorption sites remain three- and four-fold coordinated after the interaction due to the breaking of their mutual bond. Ce-O bond lengths involving the cluster-derived OH group are elongated by 0.15 Å relative to their values before water adsorption. The distances between the Ce atom at which the water-derived OH group is adsorbed and the O_C atoms with which it still shares bonds are similarly elongated. Despite this distortion of the larger nanocluster upon H_2O adsorption, the interaction is strong and favourable as shown by an adsorption energy of -1.09 eV. Similarly to the smaller nanocluster, there is a redistribution of charge with water oxygen transferring 0.3 electrons to the nanocluster and this charge is donated to the nanocluster oxygen that binds with hydrogen from water.

Figure S6 shows the PEDOS of the H_2O molecule and reduced Ce_6O_9-rutile-(110) composites in the non-interacting case (H_2O + surface) and after dissociative adsorption (H_2O-surface). In the non-interacting cases (Figure S6(a)), the water-derived O_W 2p states are well defined peaks at energies of -3.9 eV and -2.0 eV relative to the VBM (0 eV) of the TiO_2 support. For the interacting cases (Figure S6(b)) the O_W 2p-derived states overlap the O_C 2p-derived states near the VBM of the titania host. The differences in the adsorption geometries, and perhaps the underlying mechanisms driving dissociation, are reflected in the behaviour of the O_W 2p-derived states after adsorption. For dissociated water on the Ce_6O_9-rutile-(110) surface, a sharp O_W 2p-derived peak lies above the VBM because the OH group is terminal, coordinating to a single Ce site. For adsorption at the Ce_5O_8-rutile-(110) composite (see Figure 6 of main text), the O_W 2p states broaden and lie below the VBM, overlapping with O_C derived states, as in this instance the OH groups each bridge two Ce sites of the nanocluster. Comparing Figures 6(a) and 6(b), the O_W-derived states are shifted to lower energies upon dissociative adsorption. This trend is not seen in comparing Figures S6(a) and S6(b) due to the aforementioned singly coordinated OH group which results from adsorption of H_2O at the Ce_6O_9-rutile-(110) surface.

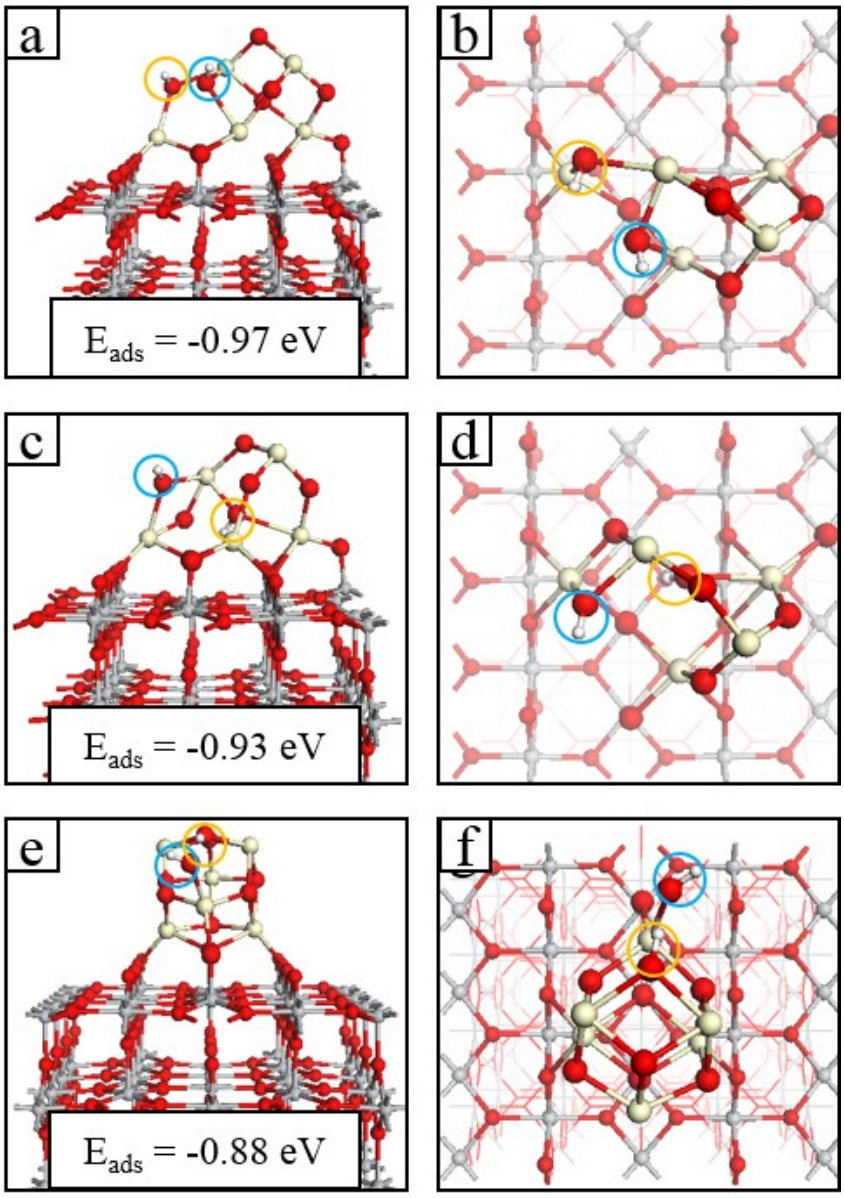

Figure S5 Relaxed atomic structure for stable configurations of H_2O adsorbed at **(a)**, **(b)**, **(c)** and **(d)** Ce_5O_8-rutile-(110) and **(e)** and **(f)** Ce_6O_9-rutile-(110). Panels on the left show side views, panels on the right show top views. Insets of panels on the left show the adsorption energies. Colour code: Ti, grey; O, red; Ce, cream; H, white.

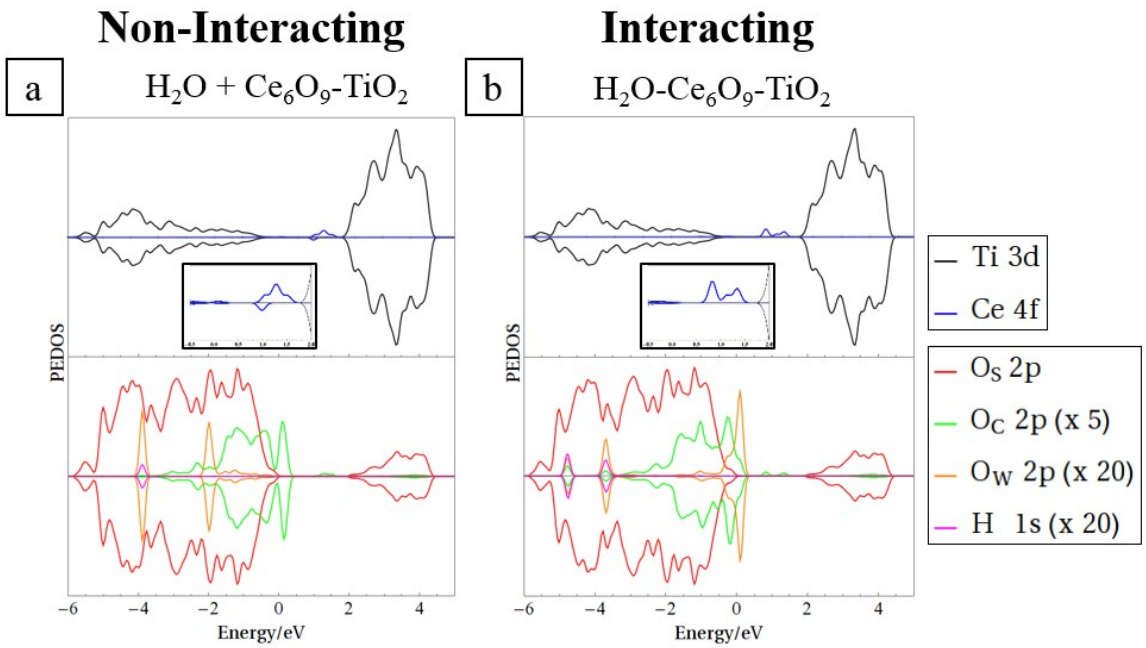

Figure S6 Spin polarized projected electron density of states (PEDOS) for **(a)** $H_2O + Ce_6O_9$-rutile-(110) (non-interacting) and **(b)** H_2O-Ce_6O_9-rutile-(110) (interacting). The top half of each panel displays Ti 3d- and Ce 4f-derived states. Bottom halves of the panels display contributions to the DOS from surface (O_S), nanocluster (O_C) and water (O_W) oxygen 2p-derived states and H 1s states. Insets in the top panels show the mid-gap Ce-derived states in the range [-0.5 eV, 2.0 eV].

The following Figures and analysis are relevant to **Section 3.5** of the main text: ***"CO_2 adsorption at the reduced nanocluster-surface composites".***

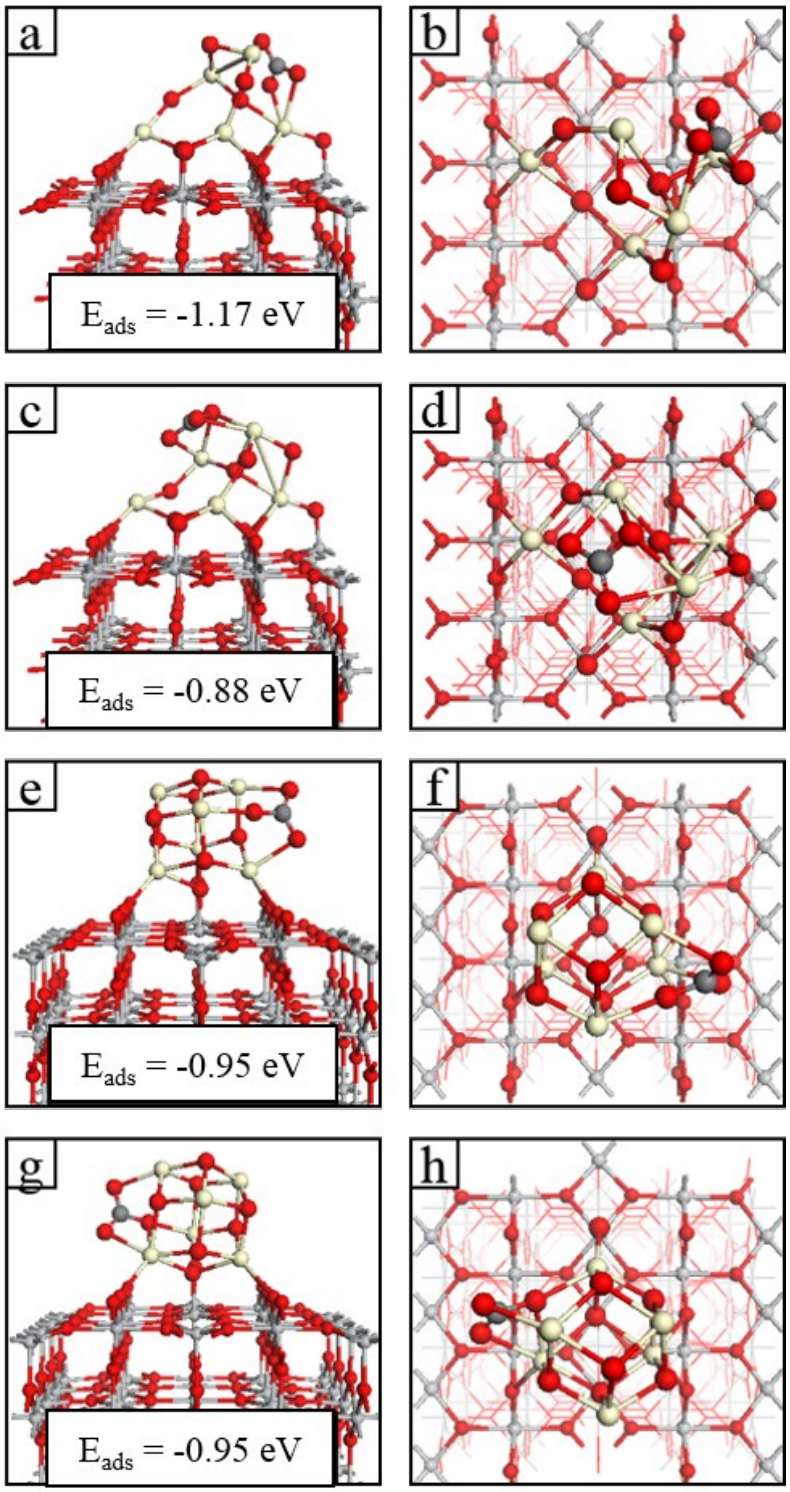

Figure S7 Relaxed atomic structure for stable configurations of CO_2 adsorbed at **(a)**, **(b)**, **(c)** and **(d)** Ce_5O_8-rutile-(110) and **(e)**, **(f)**, **(g)** and **(h)** Ce_6O_9-rutile-(110). Panels on the left show side views, panels on the right show top views. Insets of panels on the left show the adsorption energies. Colour code: Ti, grey; O, red; Ce, cream; C, dark grey.

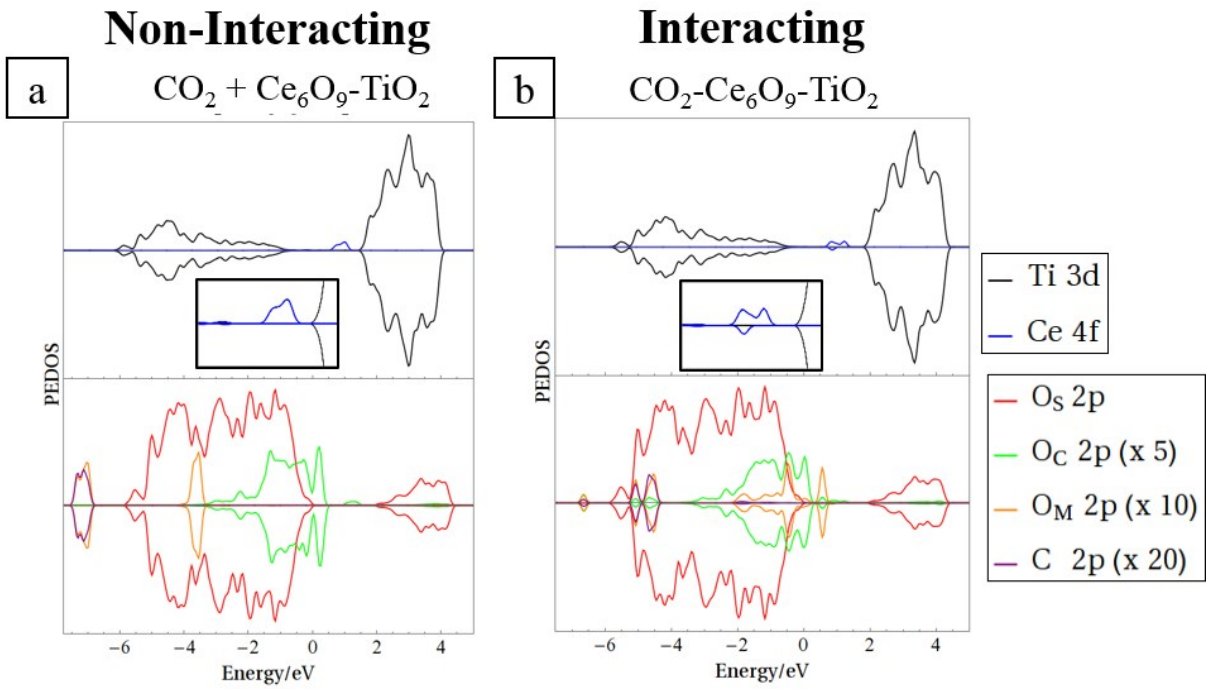

Figure S8 Spin polarized projected electron density of states (PEDOS) for **(a)** CO_2 + Ce_6O_9-rutile-(110) (non-interacting) and **(b)** CO_2-Ce_6O_9-rutile-(110) (interacting). The top half of each panel displays Ti 3d- and Ce 4f-derived states. Bottom halves of the panels display contributions to the DOS from surface (O_S), nanocluster (O_C) and CO_2 molecule (O_M) oxygen 2p-derived states and H 1s states.

Figure S8 shows the PEDOS of the CO_2 molecule and reduced Ce_6O_9-rutile-(110) composites in the non-interacting case (denoted CO_2 + surface) and after activation (denoted CO_2-surface). For the non-interacting system the molecule and surface are relaxed in the same unit cell with sufficient spatial separation such that they do not interact. In the non-interacting case (Figure S8(a)), the CO_2 molecule-derived O_M 2p states are well defined peaks at energies of -7.0 eV and -3.6 eV relative to the VBM (0 eV) of the TiO_2 support. The highest occupied molecular orbital (HOMO) of the CO_2 molecule coincides with the deepest levels of the ceria nanocluster-derived VB. This alignment of O_M 2p and O_C 2p states facilitates the interaction of the CO_2 molecule with the modified surface. For the interacting case (Figure S8(b)) the O_M 2p-derived states overlap the O_C 2p-derived states near the VBM of the titania host.

The interaction increases the gap between the occupied Ce 4f-derived states and the CBM of the TiO_2 host; i.e. the occupied Ce^{3+} states are pushed to lower energy after interaction. In addition, integrating the O_C and O_M-derived DOS lying above the TiO_2 VBM in both the non-interacting and interacting cases shows that after interaction the occupied states are driven to lower energies. These details suggest that passivation of high lying O 2p states is a factor driving the interaction of CO_2 with the reduced CeO_x-rutile-(110) composite surfaces. In particular, for both reduced composites (see also Figure 8 of the main text), the interaction of

the carbon with the nanocluster suppresses O_C-derived states at the VBM (~ 0 eV) and pushes them to lower energies (~ – 5 eV).

REFERENCES

1. M. Fronzi and M. Nolan, *ACS Omega*, 2017, **2**, 6795-6808.
2. M. Nolan, A. Iwaszuk, A. K. Lucid, J. J. Carey and M. Fronzi, *Adv. Mater.*, 2016, **28**, 5425-5446.
3. A. Iwaszuk and M. Nolan, *Phys. Chem. Chem. Phys.*, 2011, **13**, 4963-4973.
4. A. Lucid, A. Iwaszuk and M. Nolan, *Mater. Sci. Semicond. Process.*, 2014, **25**, 59-67.
5. A. Iwaszuk, P. A. Mulheran and M. Nolan, *J. Mater. Chem. A*, 2013, **1**, 2515-2525.
6. M. Fronzi, A. Iwaszuk, A. Lucid and M. Nolan, *J. Phys.: Condens. Matter*, 2016, **28**, 074006.
7. M. Fronzi, W. Daly and M. Nolan, *Appl. Catal., A:* , 2016, **521**, 240-249.